

# Super-resolution reconstruction in a computational compound-eye imaging system

Wai-San Chan · Edmund Y. Lam · Michael K. Ng ·  
Giuseppe Y. Mak

Received: 15 December 2005 / Revised: 23 March 2006 /  
Accepted: 6 June 2006 / Published online: 23 February 2007  
© Springer Science+Business Media, LLC 2007

**Abstract** From consumer electronics to biomedical applications, device miniaturization has shown to be highly desirable. This often includes reducing the size of some optical systems. However, diffraction effects impose a constraint on image quality when we simply scale down the imaging parameters. Over the past few years, compound-eye imaging system has emerged as a promising architecture in the development of compact visual systems. Because multiple low-resolution (LR) sub-images are captured, post-processing algorithms for the reconstruction of a high-resolution (HR) final image from the LR images play a critical role in affecting the image quality. In this paper, we describe and investigate the performance of a compound-eye system recently reported in the literature. We discuss both the physical construction and the mathematical model of the imaging components, followed by an application of our super-resolution algorithm in reconstructing the image. We then explore several variations of the imaging system, such as the incorporation of a phase mask in extending the depth of field, which are not possible with a traditional camera. Simulations with a versatile virtual camera system that we have built verify the feasibility of these additions, and we also report the tolerance of the compound-eye system to variations in physical parameters, such as optical aberrations, that are inevitable in actual systems.

**Keywords** Super-resolution · Compound-eye · Phase-mask

---

W.-S. Chan · E. Y. Lam (✉) · G. Y. Mak  
Department of Electrical and Electronic Engineering, The University of Hong Kong,  
Pokfulam Road, Hong Kong, Hong Kong  
e-mail: elam@eee.hku.hk

M. K. Ng  
Department of Mathematics, Hong Kong Baptist University, Kowloon Tong, Hong Kong,  
Hong Kong

## 1 Introduction

Developments in consumer electronics and biomedical instrumentations have called for miniaturization of both the electronics and the optical components. While certain traditional imaging systems with a single optical channel can be made smaller by direct down-scaling the whole system, this often comes at the expense of the image quality due to diffraction. Instead, recent developments in non-traditional image architecture have shown that a compound-eye construction can be a promising solution. In a compound-eye camera, instead of using a single large lens (or, more precisely, a set of lenses with large diameters in cascade) to form a single image of the object, it uses an array of small lenses to form multiple low-resolution (LR) sub-images. The final high-resolution (HR) image of the object is reconstructed by post-processing the sub-images. An important motivation of this novel design of an imaging system lies in the resulting system compactness.

Compound-eye imaging system design has received a lot of attention in recent years. Besides compactness, other advantages of this design includes lightness and a wide field of view. Possibility of parallel signal processing is also considered a potential of compound-eye cameras yet to be explored fully. Several research groups have designed and constructed a variety of compound-eye imaging systems (Duparré et al., 2004, 2005; Tanida et al., 2001). For example, an artificial apposition compound-eye imaging system was designed based on the apposition compound eyes of small invertebrates (Duparré et al., 2004). Although this design drastically reduces the thickness of an imaging system below 1 mm, both the resolution power and light efficiency of the system is very low as only one sample point of each sub-image is used in the reconstruction of the final image (Duparré et al., 2005). Thin Observation Module by Bound Optics TOMBO is another design of imaging system with multiple lenses. The TOMBO research team has designed, fabricated physical systems, and performed tests with their compound-eye imaging system. This system has the advantage of high sensitivity over the artificial compound-eye imaging system as the entire region of each of the sub-images is used to reconstruct the image of the object (Tanida et al., 2001). Reconstruction methods based on interpolation of pixel values have been developed, which produce images of fair quality (Kitamura et al., 2004), but improvements seem highly possible.

Low resolution and poor image quality are the most challenging issues of compound-eye imaging systems. In this paper, we present an analysis of a compound-eye system that resembles the TOMBO architecture. We describe both the physical construction and the mathematical modeling, together with our own super-resolution algorithm for image reconstruction to enhance the quality and resolution of the reconstructed image. We also consider extensions to the basic compound-eye system, such as the inclusion of a phase mask in some of the optical paths, to make use of the extra flexibility due to multiple optical paths. Simulation experiments are also conducted to investigate the performance of our methods. These are described as follows. In Sect. 2, we describe the compound-eye imaging model of our concern. In Sect. 3, the super-resolution reconstruction algorithm is explained. Simulation results which investigate the performance of super-resolution reconstruction, the tolerance of the system to aberrations, and the incorporation of phase masks to extend the depth-of-field are discussed in Sect. 4. Finally, concluding remarks are provided in Sect. 5.

## 2 Architectures of computational compound-eye imaging systems

In general, compound-eye imaging systems belong to an emerging area called “integrated computational imaging system,” which takes into account the optics, optoelectronics, and image processing as a whole in image formation and processing rather than as independent modules as in traditional imaging system (Mait, Athale, & van der Gracht, 2003). The optics part appears at the front end, and involves how light from the target objects is converged and gathered. In a compound-eye system, the task is largely shared among multiple small lenses. The optical module often introduces a degradation due to the effects of diffraction and lens aberrations, which can be compensated in part in the image processing (Castleman, 1996). Next in the system comes the optoelectronics part, which involves how the optical information conveyed by the optics part is collected. The optoelectronics module usually consists of one or more arrays of photosensitive cells, whose sizes and arrangements are crucial to an effective collection of optical information which is to be utilized by the image-processing part of the system. The image-processing module attempts to restore a fine image of the target objects from the collected optical information. This may involve deblurring and, in the case of compound-eye systems, image reconstruction from multiple LR sub-images.

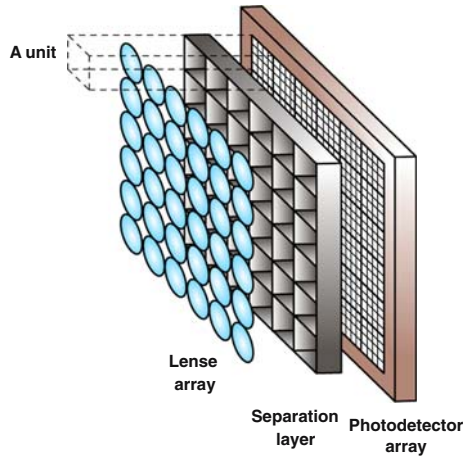
Several research groups have designed novel architectures of compound eye cameras (Duparré, Dannberg, Schreiber, Bräuer, & Tünnermann, 2005; Duparré et al., 2005; Hornsey et al., 2004; Krishnasamy et al., 2004; Neumann, Fermüller, Aloimonos, & Brajovic, 2004). For instance, one architecture was designed based on the apposition compound-eyes of small invertebrates (Duparré et al., 2005). The architecture consists of a large array of small lenses (which we refer to as lenslets or microlenses in this paper) and a pinhole array on top of a sensor array on the focal plane of the lenslets. Each lenslet together with a pinhole forms an optical channel, which corresponds to a small field angle in the object space. This architecture does not require complex image processing and allows the system to become extremely compact, at the expense of the resolution of the image and sensitivity of the system. Another possible architecture of compound-eye imaging system consists of several microlens arrays which are of different pitches, and an image sensor plane (Duparré et al., 2005). Each optical channel has its own optical axis which is tilted from each other so that all microimages are obtained from a different viewing directions but with certain overlap. The overall image is obtained by combining all the microimages. This architecture has the merit of the possibility of high magnification, but a drawback of a much higher system complexity.

Figure 1 shows another possible architecture of a compound-eye system (Tanida et al., 2001). This is the baseline system that we are considering in this paper. In this system, there is a lens array which is composed of  $N \times N$  microlenses, and a photodetector array which consists of  $T \times T$  photosensitive cells.  $T$  is in general much larger than  $N$ ; therefore, each microlens corresponds to  $\beta \times \beta$  cells, where

$$\beta = \frac{T}{N}. \quad (1)$$

A microlens together with its array of photosensitive cells form an imaging unit. Each imaging unit of the compound-eye imaging system generates an LR sub-image of the object. To avoid cross-talk between the individual sub-images, a separation layer

**Fig. 1** The computational compound-eye system (Tanida et al., 2001)



which consists of partition blocks is often placed between the lens array and the photodetector array.

After image capture, the remaining task is to reconstruct the HR image from the collection of LR sub-images. Different methods have been proposed for this step, including the sampling method (Tanida et al., 2001) and the pixel rearrangement method (Kitamura et al., 2004). The latter method shows a significant improvement over the former, but still there is room for improvement in terms of image quality. In particular, this compound-eye architecture allows the possibility of image reconstruction by a particular implementation of our super-resolution algorithm. Indeed, provided that there are sub-pixel displacements in all the sub-images so that there are no redundant sub-images, super-resolution can be employed to reconstruct a HR image from the multiple LR sub-images (Bose & Boo, 1998; Ng & Bose, 2003).

The working principle of the computational compound-eye imaging system is shown in Fig. 2. Furthermore, in this architecture, each imaging unit of the system has its own optical path and image formation of the target object. For this reason, there is also a possibility of greater flexibility in each optical path. Deliberate introduction of path length errors with restoration may enhance the capabilities of the system. For instance, integration of wavefront coding in a channel can help increase the depth of field of the image (Dowski & Cathey, 1994). On the other hand, inadvertent introduction of errors due to fabrication is also expected. Fabrication errors include deviation of focal lengths of the microlenses, aberrations, and assembly misalignment of the individual components. The effects of the fabrication errors are to be minimized by the post-processing algorithm of the system. We consider all these variations of our baseline compound-eye system, which we also address later on in this paper.

### 3 Image reconstruction by super-resolution

In this section, we describe the mathematical modeling of the optical system and the super-resolution algorithm we used in the reconstruction process. Because we can assume linearity in the entire electro-optical system, matrix equations are used in describing the effects of various components (Elad & Feuer, 1997). All the images

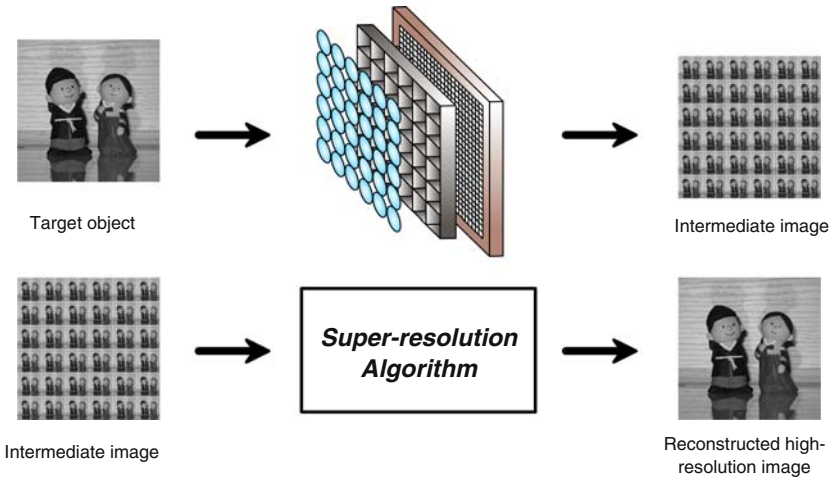


**Fig. 2** Diagram showing the flow of the computational compound-eye imaging system

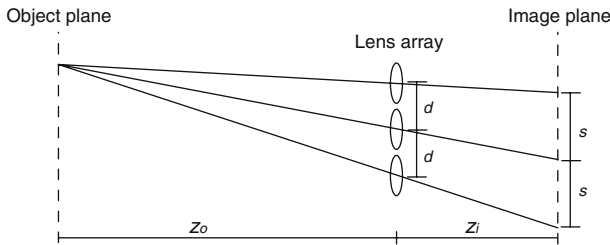


**Fig. 3** Diagram showing the relative amount of displacements of the sub-images produced by the individual lenses in the lens array

are represented by vectors formed by lexicographical ordering of the image pixels. The target object is regarded as the HR image on which a series of operations are performed in the imaging process to produce the LR sub-images. Since each imaging unit operates individually in its own optical path, under the assumption that there is no cross-talk between the sub-images, the formation of each sub-image can be modeled independently from one another in its own channel. Consequently, a compound-eye system with  $N \times N$  lenses gives  $N^2$  optical channels and thus  $N^2$  sub-images.

Let the lens on the first row and first column be the reference lens, and the coordinates of its corresponding sub-image be the reference frame. Furthermore, assume both the horizontal and vertical separations of two neighboring lenses are the same, which we denote as  $d$ . We also label the target HR image as  $\mathbf{f}$ , which is of length  $M^2$ . Now consider the modeling of the sub-image  $\mathbf{i}_k$ , which is of length  $\beta^2$ , produced by the lens in the  $p$ th row and  $q$ th column.  $k$  is the index of the image, and is related to  $p$  and  $q$  by

$$k = (p - 1)N + q. \tag{2}$$

We can derive the displacement of the images with respect to the reference image by taking into account the optical system parameters. Consider Fig. 3, which is a simplified view of the image formation process. As the  $k$ th lens is displaced vertically

and horizontally from the reference lens by  $(p - 1)d$  and  $(q - 1)d$ , respectively, the corresponding sub-image formed is shifted away from the reference frame by

$$s_v = (p - 1)[(m + 1)d - \beta w] \quad \text{and} \quad s_u = (q - 1)[(m + 1)d - \beta w] \quad (3)$$

in the vertical and horizontal directions, respectively, where  $w$  is the pixel width and  $m$  is the magnification of the system given by

$$m = \frac{z_i}{z_o} \quad (4)$$

with  $z_i$  as the image distance and  $z_o$  as the object distance. Mathematically, this image displacement can be modeled with a shifting matrix  $S_k$ . In practice, the amount of shifting can either be estimated from the imaging system parameters, or from the captured sub-images themselves with techniques such as cross-correlation (Kitamura et al., 2004).

The lens and the finite sizes of the photosensitive cells often introduce blurring to the sub-images. The former causes a loss of high frequency due to the finite size of the aperture, while the latter gives rise to a sum of light flux within the area captured by the individual photodetector. Both can be considered lowpass filters. Due to the space-invariant nature of these two operations, the effects can be convolved together, and ultimately represented by a single blurring matrix  $B_k$  for each optical channel. Meanwhile, since the sub-image is of lower resolution than the HR image, down-sampling has to be performed, which is represented by the down-sampling matrix  $D_k$ . Finally, noise is added to the sub-image due to noise of the photosensitive cells and quantization. This is represented by the noise vector  $\mathbf{v}_k$ . The modeling is shown schematically in the block diagram in Fig. 4.

The various steps can be combined together to form the image formation equations

$$\mathbf{i}_k = D_k B_k S_k \mathbf{f} + \mathbf{v}_k, \quad k = 1, 2, \dots, N^2. \quad (5)$$

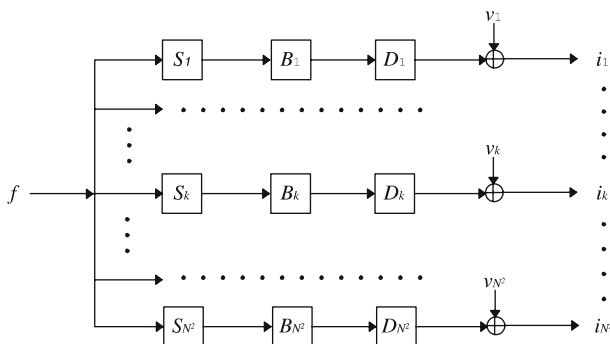


**Fig. 4** Block diagram representation of the compound-eye imaging system

Since there are  $N^2$  channels, there are  $N^2$  equations for the set of LR sub-images  $\{\mathbf{i}_1, \mathbf{i}_2, \dots, \mathbf{i}_{N^2}\}$ . Stacking all the equations results in a single matrix equation given by

$$\begin{bmatrix} \mathbf{i}_1 \\ \vdots \\ \mathbf{i}_k \\ \vdots \\ \mathbf{i}_{N^2} \end{bmatrix} = \begin{bmatrix} D_1 B_1 S_1 \\ \vdots \\ D_k B_k S_k \\ \vdots \\ D_{N^2} B_{N^2} S_{N^2} \end{bmatrix} \mathbf{f} + \begin{bmatrix} \mathbf{v}_1 \\ \vdots \\ \mathbf{v}_k \\ \vdots \\ \mathbf{v}_{N^2} \end{bmatrix}. \tag{6}$$

We can write it more simply as

$$\mathbf{i} = H\mathbf{f} + \mathbf{v}, \tag{7}$$

where  $H$  is called the blurring matrix of the whole system, and  $\mathbf{v}$  is the noise vector. Note that  $H$  is a function of all the blurring, shifting, and downsampling in each of the channels. This is in general space-variant, making this different from a traditional image restoration problem (Katsaggelos, 1991).

Solving  $\mathbf{f}$  in Eq. 6 in fact represents a super-resolution problem, because it is of a higher resolution than the available LR images. Since this is an ill-conditioned problem, regularization is necessary. The general framework of the solution  $\hat{\mathbf{f}}$  can be expressed as (Bose & Boo, 1998)

$$\hat{\mathbf{f}} = \arg \min_{\mathbf{f}} \left\{ \|H\mathbf{f} - \mathbf{i}\|^2 + \alpha \mathbf{R}(\mathbf{f}) \right\}, \tag{8}$$

where the function  $\mathbf{R}(\mathbf{f})$  measures the regularity of  $\mathbf{f}$  and  $\alpha$  is the regularization parameter which controls the regularity of the solution. The  $L_2$  and  $H_1$  regularization functionals  $\mathbf{R}(\mathbf{f}) = \|\mathbf{f}\|_2^2$  and  $\mathbf{R}(\mathbf{f}) = \|L\mathbf{f}\|_2^2$  are used where  $L$  is the first-order differential operator. Using the Tikhonov regularization, the problem becomes

$$(H^T H + \alpha R) \mathbf{f} = H^T \mathbf{i}, \tag{9}$$

where  $R$  is the discretization matrix corresponding to the regularization functional  $\mathbf{R}(\mathbf{f})$  (Ng & Bose, 2003). We solve this large linear system iteratively by the conjugate gradient method (Ng & Bose, 2002; Ng & Yip, 2001). Although this is often a very effective optimization technique, the convergence rate can be very slow if the condition number of the matrix  $(H^T H + \alpha R)$  is large. Preconditioning of the system can speed up the convergence rate (Ng & Bose, 2003). The preconditioned system to be solved is

$$P^{-1} (H^T H + \alpha R) \mathbf{f} = P^{-1} H^T \mathbf{i}, \tag{10}$$

where  $P$  is the preconditioner. In our algorithm, cosine transform preconditioners are used to increase the computational speed for the reconstruction process. We refer the readers to a previous publication for more details (Ng, Chan, Chan, & Yip, 2000).

What we have described so far are the basic setup and modeling of our compound-eye imaging system. For practical applications, two extensions are possible and should also be considered here. First, fabricating such an array of lenses with high precision can be rather costly. There may often be variations in imaging parameters along different optical paths, such as differences in focal length due to slight changes in the curvature of the lenses. However, since each of the optical path is

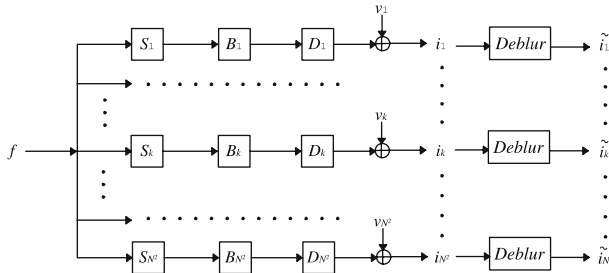


**Fig. 5** Deblurring of the sub-images is performed before the sub-images are fed into the super-resolution reconstruction algorithm

essentially independent from each other, a post-processing step to deblur each of the channel is possible. Figure 5 shows schematically how the post-processing compensates the variation in the focal lengths of the lenses. The sub-images are deblurred (for instance, restored from defocus) before they are fed to the super-resolution reconstruction algorithm (Lam, 2002; Lam & Goodman, 1998). On the other hand, for certain applications, estimating the blurs in each of the channels may be impossible or very costly. It would also be interesting from a hardware design perspective to explore how much variation is possible before severe degradation to image quality occurs, in the event that we do not perform individual deblurring but use Eq. 10 to find **f**. We provide some simulation results in the next section to address this problem.

The second extension can be considered the dual to the first one described above: instead of trying to restore certain blurring introduced inadvertently, we deliberately introduce some aberrations to some of the optical channels and restore them appropriately after image capture. This idea may appear peculiar at first, but it underlines the work known as wavefront coding or pupil phase engineering (Castro & Ojeda-Castañeda, 2004; Dowski & Cathey, 1995; Prasad, Torgersen, Pauca, Plemmons, & van der Gracht, 2004; Sherif, Cathey, & Dowski, 2004). They have demonstrated that by introducing some particular aberrations, such as a cubic-phase mask in front of a lens, the image would appear very blurry at capture. These aberrations cause path-length errors in the wavefront. However, information has actually been preserved well for a large range of focus. After proper digital restoration, a sharp image can be obtained. In essence, this extends the depth-of-field of the imaging system at the expense of more computation. While the bulk of this study has centered on a single-lens system, we see that it can be extended to our compound-eye imaging system. In particular, with multiple optical channels, they can actually acquire different information when some of the channels are equipped with phase masks. Figure 6 shows the incorporation of the phase-mask operators in the compound-eye system model. The matrix equation for the *k*th channel becomes

$$\mathbf{i}_k = D_k M_k B_k S_k \mathbf{f} + \mathbf{v}_k, \tag{11}$$

where  $M_k$  is the matrix for the phase-mask operator. For those channels that do not consist of a phase mask, we can set  $M_k$  to be the identity matrix. Accordingly, we have the matrix equation for the whole system as

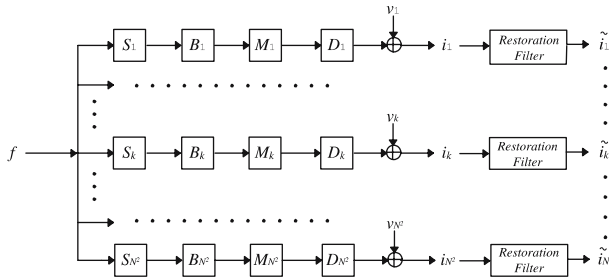


**Fig. 6** Block diagram representation of the compound-eye imaging system with the incorporation of phase masks

$$\begin{bmatrix} \mathbf{i}_1 \\ \vdots \\ \mathbf{i}_k \\ \vdots \\ \mathbf{i}_{N^2} \end{bmatrix} = \begin{bmatrix} D_1 M_1 B_1 S_1 \\ \vdots \\ D_k M_k B_k S_k \\ \vdots \\ D_{N^2} M_{N^2} B_{N^2} S_{N^2} \end{bmatrix} \mathbf{f} + \begin{bmatrix} \mathbf{v}_1 \\ \vdots \\ \mathbf{v}_k \\ \vdots \\ \mathbf{v}_{N^2} \end{bmatrix}. \tag{12}$$

We obtain the matrix equation for the system as

$$\mathbf{i} = \tilde{H}\mathbf{f} + \mathbf{v}, \tag{13}$$

where  $\tilde{H}$  is the phase-mask-incorporated blurring matrix.  $\mathbf{f}$  can be solved by the techniques of minimization and regularization in the same fashion as discussed earlier in this section. Consequently, we should obtain a HR image with an extended depth of field.

### 4 Simulation

A virtual camera is built to investigate the performance of a computational compound-eye system with super-resolution reconstruction. The virtual camera can simulate an  $N \times N$  compound-eye system where  $N$  can take on any positive integer value. Random aberrations can be simulated in the system. In addition, phase masks can be inserted into the system. A number of parameters of the virtual camera can be set, for example, the focal lengths of the lenses, the pixel dimensions, the noise type, and noise amount. Furthermore, instead of using geometric optics assumption in the image formation model, it takes into account the effect of diffraction on the images produced. A screenshot of the virtual camera is shown in Fig. 7.

For a diffraction limited system, the impulse response, or equivalently the point-spread function (PSF), of an in-focus image is given by the Fraunhofer diffraction pattern of the lens aperture. This is give by

$$h(u, v) = \frac{A}{\lambda z_i} \int_{-\infty}^{\infty} \int_{-\infty}^{\infty} P(x, y) \exp \left\{ -j \frac{2\pi}{\lambda z_i} (ux + vy) \right\} dx dy, \tag{14}$$

where the pupil function  $P$  is unity inside and zero outside the projected aperture,  $A$  is a constant amplitude,  $z_i$  the image distance,  $\lambda$  the wavelength of the illumination, and  $(x, y)$  are coordinates in the plane of the exit pupil. We can see that the effect of

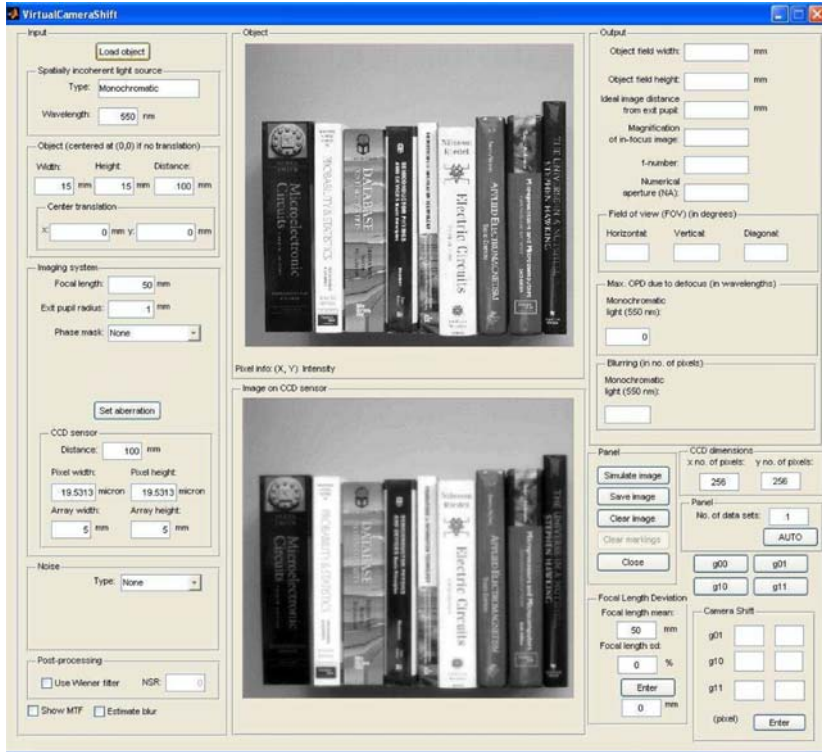


Fig. 7 A screen shot of the virtual camera

diffraction is actually realized by convolving the object with the Fraunhofer diffraction pattern of the lens aperture, which leads to a loss of fine details of the object (Goodman, 1996).

The algorithm of the virtual camera is mainly based on the theory of Fourier optics. The object and image is related in the frequency domain by the following equation:

$$G_i(f_X, f_Y) = \mathcal{H}(f_X, f_Y)G_g(f_X, f_Y), \tag{15}$$

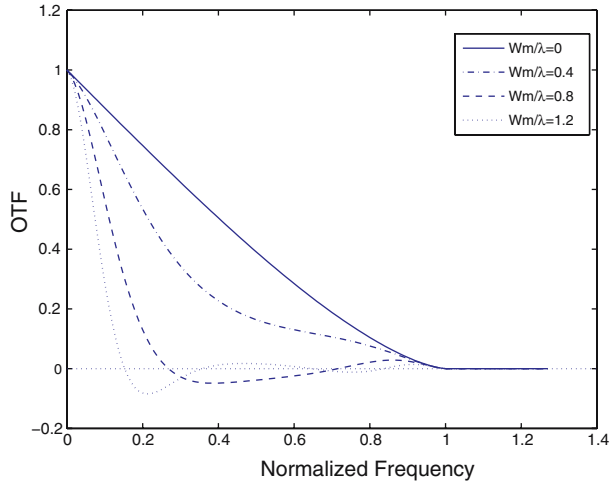
where  $G_i(f_X, f_Y)$  and  $G_g(f_X, f_Y)$  are the normalized frequency spectra of the image intensity and the object intensity, respectively.  $\mathcal{H}(f_X, f_Y)$  is the optical transfer function (OTF) given by

$$\mathcal{H}(f_X, f_Y) = \frac{\int_{-\infty}^{\infty} \int_{-\infty}^{\infty} H\left(x + \frac{f_X}{2}, y + \frac{f_Y}{2}\right) H^*\left(x - \frac{f_X}{2}, y - \frac{f_Y}{2}\right) dx dy}{\int_{-\infty}^{\infty} \int_{-\infty}^{\infty} |H(x, y)|^2 dx dy}, \tag{16}$$

where  $H$  is the Fourier transform of the PSF  $h(u, v)$  of the optical system given by Eq. 14. When the system is diffraction-limited with no aberrations, the spectrum of the PSF can be written as a scaled version of the spectrum of the pupil function  $P$ :

$$H(f_X, f_Y) = P(\lambda z_i f_X, \lambda z_i f_Y). \tag{17}$$

**Fig. 8** Cross section of the OTF with normalized frequency



When aberrations exist, we can also find the OTF by inserting the path-length error  $W(x, y)$  appropriately. The spectrum of the PSF then becomes

$$H(f_X, f_Y) = P(\lambda z_i f_X, \lambda z_i f_Y) \exp \{jkW(\lambda z_i f_X, \lambda z_i f_Y)\}. \tag{18}$$

Equation 16 can then be used to calculate the OTF. Figure 8 shows a cross section of the OTF with the normalized frequency for different normalized path-length errors (Lam & Goodman, 1998). It can be observed that due to diffraction, even for an aberration-free in-focus image, there is attenuation of the high frequency components. Moreover, beyond the cutoff frequency, all frequency components are lost. The extent of high-frequency attenuation increases with increasing focusing error, which is measured by the quantity  $W_m/\lambda$  (Goodman, 1996).

Simulations have been performed to first investigate the performance of our super-resolution algorithm on system with no aberrations. Nevertheless, since it is unlikely that the lenses in a practical compound-eye system all have the exact required focal length, simulations have been done to investigate the effects of deviation of focal lengths of the lenses on the quality of the reconstructed image. To demonstrate the flexibility in the optical channels, simulations have been done to investigate the ability of using phase-masks in the compound-eye system to increase the depth-of-field. For simplicity, we simulate a compound-eye system with  $2 \times 2$  imaging units.

#### 4.1 System with no aberrations

An imaging system with no aberrations is first investigated. Under this setting, all the lenses in the lens array have the exact required value of focal length (thus all four sub-images captured are in-focus) and that there are no other kinds of aberrations. It is worth noting that although the sub-images are in focus, fine details of the object are attenuated due to the effect of diffraction. Figure 9 shows the simulation result, where the first column shows one of the sub-images and the second column shows the image reconstructed by super-resolution. The images in the latter are noticeably sharper, as expected. As a comparison, we also show the result with the “pixel rearrangement method” as suggested in (Kitamura et al., 2004) for comparison. Again, in terms of

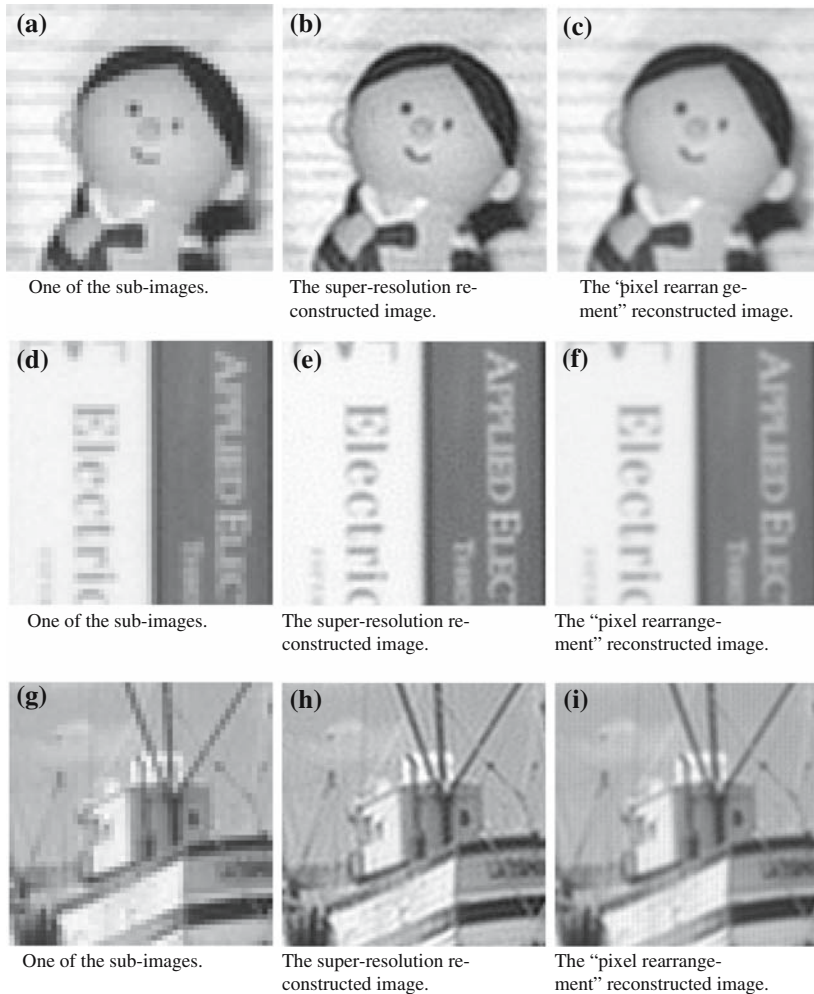


**Fig. 9** Simulation results from the virtual camera with super-resolution reconstruction

visual image quality, our reconstructed images outperform the pixel rearrangement method. We also compare the two schemes in terms of their signal-to-noise ratios (SNR). Some data are shown in Table 1. In general, the SNR of the super-resolution reconstructed images is about 25 dB, which is about 0.5 dB higher than those obtained by the “pixel rearrangement method.”

#### 4.2 System with lenses which have focal length errors

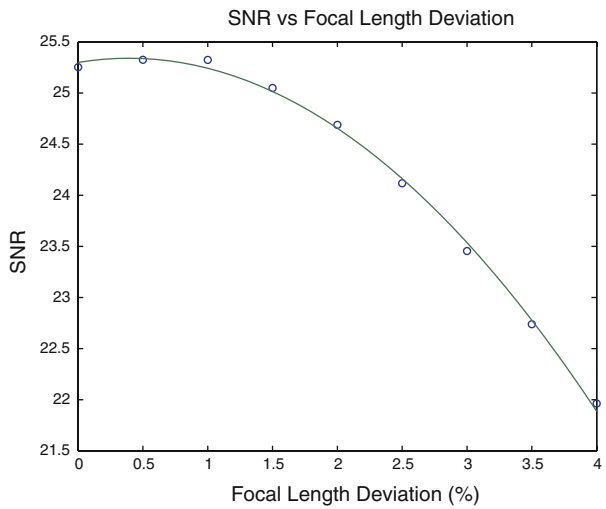
When the lenses do not have the exact focal lengths required, focusing errors will be present. This results in path-length error which is given by

$$W(x, y) = -\frac{1}{2} \left( \frac{1}{z_a} - \frac{1}{z_i} \right) (x^2 + y^2), \quad (19)$$

**Table 1** Comparison of the SNRs of the reconstructed images obtained by the “Pixel Rearrangement Method” and “Super-resolution Reconstruction”

Target object	SNR (dB)	
	Reconstruction method	
	Super-resolution reconstruction	Pixel rearrangement
Bridge	18.1	17.7
Boat	22.0	21.4
Couple	26.0	25.6
Books	18.4	17.9

**Fig. 10** SNR against deviation of focal lengths



where  $z_i$  and  $z_a$  are the ideal and actual distance of the focusing plane from the lens, respectively, and  $(x, y)$  denotes the coordinates at the exit pupil.

In the experiments which study the effects of focal length deviation on the quality of the reconstructed images, the focal lengths of the four lenses of the virtual camera were assigned by generating a random focal length  $f$  following a normal distribution with a mean  $f_m$  and standard deviation  $\sigma$ . To avoid a large error which may be unrealistic in practice, any  $f$  generated which deviated from  $f_m$  by more than  $2\sigma$  were discarded. The percentage of focal length deviation is calculated by

$$\frac{\sigma}{f_m} \times 100\% \tag{20}$$

The four sub-images obtained from the virtual camera were used to reconstruct the HR image by our super-resolution algorithm. The SNR of the reconstructed image was then measured. Simulations were done with different percentage of focal length deviation. The results obtained were plotted and shown in Fig. 10. Note that each data point was obtained by averaging the results of 30 data sets. We can see that when the focal length deviation is within 1%, there is negligible change in the SNR. When it is about 2%, there is only about 1 dB loss. However, at 4% deviation, the loss is as much as 3 dB.

The numerical results correspond well to the visual image quality shown in Fig. 11 the reconstructed image shows acceptable visual quality when the deviation in focal

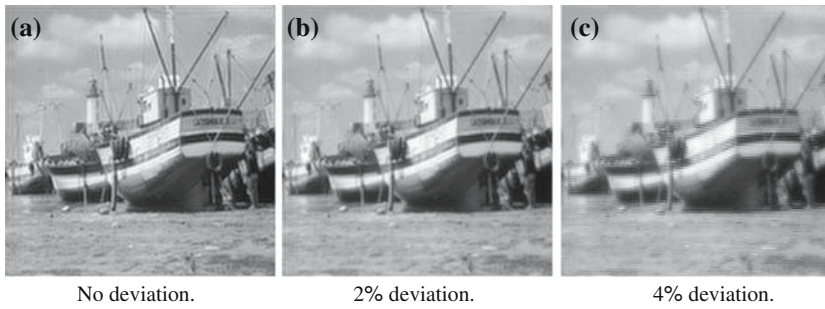


**Fig. 11** Reconstructed images with various percentage of deviation in focal length

length is about 2%. However, when the deviation in focal length extends to about 4%, artifacts becomes obvious. The numerical and the visual images together suggest that the compound-eye system is tolerant to small focal length deviations, but dedicated restoration like that proposed in Fig. 5 is necessary for large deviations.

#### 4.3 System with phase masks

In this section, we investigate the use of phase masks together with restoration filters in extending the depth-of-field of the imaging system. In our experiment, cubic phase masks are used. When we placed a cubic phase mask in front of a lens, we are deliberately introducing a path-length error which is given by

$$W(x, y) = \exp \left\{ j \frac{\alpha}{R^3} (x^3 + y^3) \right\}, \quad (21)$$

where  $\alpha$  is a constant that controls the phase deviation. Wiener Filter is used as the restoration filter in our experiment. It is give by

$$R(f_X, f_Y) = \frac{\mathcal{H}^*(f_X, f_Y)}{|\mathcal{H}(f_X, f_Y)|^2 + \frac{\Phi_v(f_X, f_Y)}{\Phi_i(f_X, f_Y)}} \quad (22)$$

in the frequency domain where  $\mathcal{H}$  is the OTF of the individual optical channel,  $\Phi_i(f_X, f_Y)$  and  $\Phi_v(f_X, f_Y)$  are the power spectra of the undegraded image and noise, respectively. In our simulated compound-eye system, there are four optical channels. In this simulation, four cubic phase masks are incorporated into the system, with each lens being associated with one cubic phase mask. Three scenes with spatial-varying depth scene are created. Figure 12 compares the reconstructed images obtained from a system without using cubic phase masks (left column) and those obtained from a system with an incorporation of four phase masks after restoration by Wiener filters (right column). In the first, second and third rows, the book is placed at distances which is 10, 20 and 30% shorter than the idea image distance, respectively. The cup is placed at the ideal image distance for all the three cases. It is clear that while some parts of the reconstructed images obtained from the system without phase masks are out-of-focus, the phase masks-incorporated system can bring the whole scene with different depths into focus. This demonstrates the capability of cubic phase masks in extending the depth-of-field in a compound-eye system .

Since there are multiple optical channels in a compound-eye system, there is a possibility of incorporating a different number of phase masks into the system.

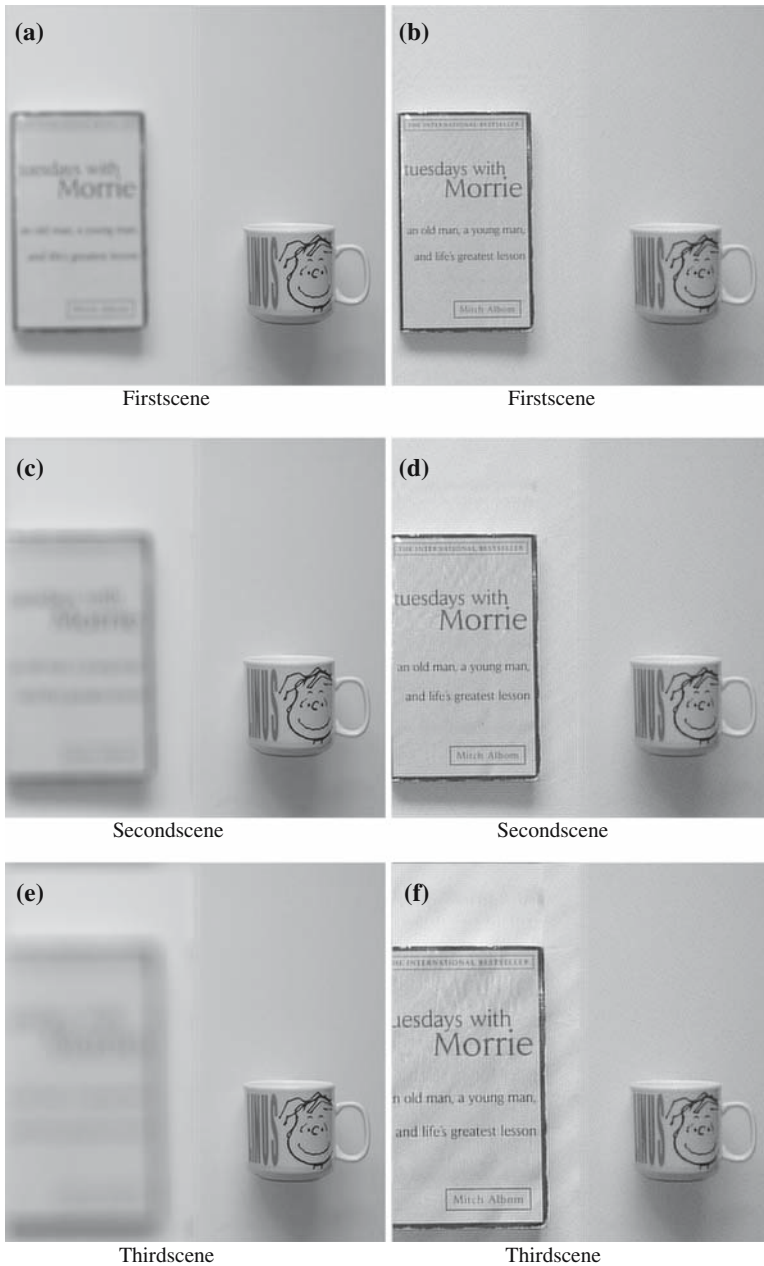


**Fig. 12** Reconstructed images from scenes with spatially varying depths

Figure 13 shows the reconstructed images obtained from systems with different number of phase masks incorporated to them. It can be observed that the more the optical channels incorporated with a phase mask, the better the quality of the reconstructed image is. This shows a trade off between the number of phase masks, which translates to cost, and the image quality. It should be noted that if only some of

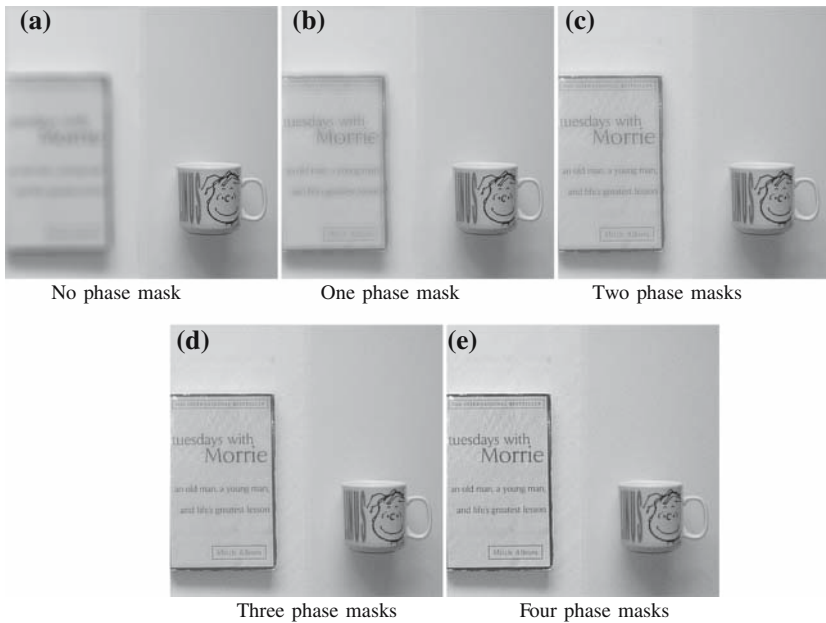


**Fig. 13** Reconstructed images with different numbers of phase masks incorporated into the compound-eye system

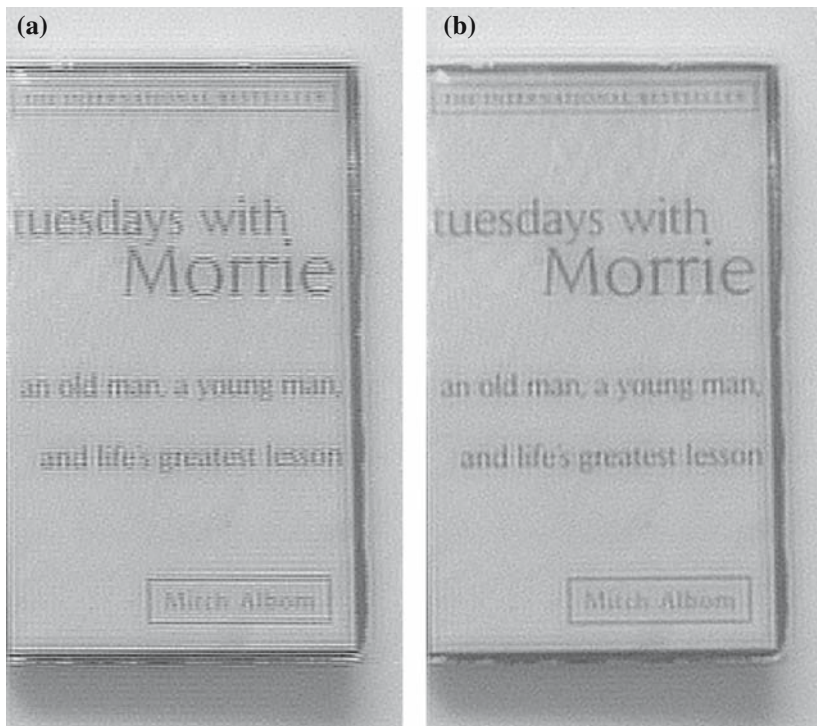
the optical channels are incorporated with phase masks, there is an issue of in which channels the phase masks should be placed. In our case of four optical channels, only the case for two phase masks should be of concern since other possibilities of positioning of the phase masks are symmetric for different number of phase masks. In the case for two phase masks inserted into two out of four of the optical channels, two ways are possible:

1. placing in side-by-side channels, or
2. placing in diagonal channels.

Figure 14 compares the two cases. It can be observed that the system with phase masks placed in diagonal channels gives images with better visual quality than that produced by the system with phase masks placed in side-by-side channels.

## 5 Conclusion

We have established and investigated a computational compound-eye imaging system with super-resolution reconstruction. Simulation results demonstrated the feasibility of the implementation of our super-resolution algorithm on image reconstruction of the compound-eye imaging system. The current system shows tolerance in focal length deviation of the lenses to some extent. Depth-of-field of the compound-eye system has been extended under the incorporation of cubic phase masks accompanied by Wiener filter restoration to the system.



Phase masks placed in side-by-side channels.

Phase masks placed in diagonal channels.

**Fig. 14** Reconstructed images with two phase masks incorporated into the compound-eye system

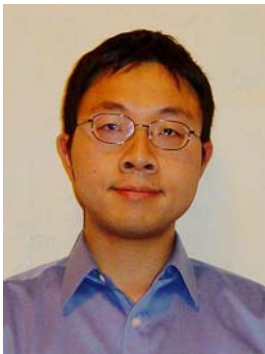
**Acknowledgements** The work described in this paper was partially supported by a grant from the Research Grants Council of the Hong Kong Special Administrative Region, China (Project Number 714305).

## References

- Bose, N. K., & Boo, K. J. (1998). High-resolution image reconstruction with multisensors. *International Journal of Imaging Systems and Technology*, 9(4), 294–304.
- Castleman, K. R. (1996). *Digital image processing*. Englewood, Cliffs, NJ: Prentice Hall.
- Castro, A., & Ojeda-Castañeda, J. (2004). Asymmetric phase masks for extended depth of field. *Applied Optics*, 43(17), 3474–3479.
- Dowski, E. R. Jr., & Cathey, W. T. (1994). Single-lens single-image incoherent passive-ranging systems. *Applied Optics*, 33(29), 6762–6773.
- Dowski, E. R. Jr., & Cathey, W. T. (1995). Extended depth of field through wave-front coding. *Applied Optics*, 34(11), 1859–1866.
- Duparré, J., Dannberg, P., Schreiber, P., Bräuer, A., & Tünnermann, A. (2005). Thin compound eye camera. *Applied Optics*, 44(15), 2949–2956.
- Duparré, J., Schreiber, P., Dannberg, P., Scharf, T., Pelli, P., Völkel, R., Herzig, H.-P., & Bräuer, A. (2004). Artificial compound eyes—different concepts and their application to ultra flat image acquisition sensors. In: *MOEMS and miniaturized systems IV, ser. proceedings of the SPIE*, San Jose, California, USA, Vol. 5346, pp. 89–100.
- Duparré, J., Schreiber, P., Matthes, A., Pshenay-Severin, E., Bräuer, A., & Tünnermann, A. (2005). Microoptical telescope compound eye. *Optics Express*, 13(3), 889–903.

- Elad, M., & Feuer, A. (1997). Restoration of a single superresolution image from several blurred, noisy, and undersampled measured images. *IEEE Transactions on Image Processing*, 6(12), 1646–1658.
- Goodman, J. W. (1996). *Introduction to fourier optics* (2nd ed.). New York: McGraw-Hill.
- Hornsey, R., Thomas, P., Wong, W., Pepic, S., Yip, K., & Krishnasamy, R. (2004). Electronic compound-eye image sensor: Construction and calibration. In: *Proceedings of the IS&T/SPIE symposium on electronic imaging 2004*. Niagara Falls, Ontario, Canada.
- Katsaggelos, A. K. (1991). *Digital image restoration*. New York: Springer.
- Kitamura, Y., Showgenji, R., Yamada, K., Miyatake, S., Miyamoto, M., Morimoto, T., Masaki, Y., Kondou, N., Miyazaki, D., & Tanida, J. (2004). Reconstruction of a high-resolution image on a compound-eye image-capturing system. *Applied Optics*, 43(8), 1719–1727.
- Krishnasamy, R., Wong, W., Shen, E., Pepic, S., Hornsey, R., & Thomas, P. (2004). High precision target tracking with a compound-eye image sensor. In: *Canadian conference on electrical and computer engineering 2004*, San Jose, California, USA.
- Lam, E. Y. (2002). Digital restoration of defocused images in the wavelet domain. *Applied Optics*, 41(23), 4806–4811.
- Lam, E. Y., & Goodman, J. W. (1998). Discrete cosine transform domain restoration of defocused images. *Applied Optics*, 37(26), 6213–6218.
- Mait, J. N., Athale, R., & van der Gracht, J. (2003). Evolutionary paths in imaging and recent trends. *Optics Express*, 11(18), 2093–2101.
- Neumann, J., Fermüller, C., Aloimonos, Y., & Brajovic, V. (2004). Compound eye sensor for 3D ego motion estimation. In: *Proceedings of the IEEE/RSJ international conference on intelligent robots and systems (IROS '04)*, IEEE.
- Ng, M., & Bose, N. K. (2002). Analysis of displacement errors in high-resolution image reconstruction with multisensors. *IEEE Transactions on Circuits and Systems I*, 49, 806–813.
- Ng, M. K., & Bose, N. K. (2003). Mathematical analysis of super-resolution methodology. *IEEE Signal Processing Magazine*, 20(3), 62–74.
- Ng, M. K., Chan, R. H., Chan, T. F., Yip, A. M. (2000). Cosine transform preconditioners for high resolution image reconstruction. *Linear Algebra and Its Applications*, 316(1–3), 89–104.
- Ng, M., & Yip, A. (2001). A fast MAP algorithm for high-resolution image reconstruction with multisensors. *Multidimensional Systems and Signal Processing*, 12(2), 143–164.
- Prasad, S., Torgersen, T., Pauca, P., Plemmons, R., & van der Gracht, J. (2004). High-resolution imaging using integrated optical systems. *International Journal on Imaging Systems and Technology*, 14(2), 67–74.
- Sherif, S. S., Cathey, W. T., & Dowski, E. R. (2004). Phase plate to extend the depth of field of incoherent hybrid imaging systems. *Applied Optics*, 43(13), 2709–2721.
- Tanida, J., Kumagai, T., Yamada, K., Miyatake, S., Ishida, K., Morimoto, T., Kondou, N., Miyazaki, D., & Ichioka, Y. (2001). Thin observation module by bound optics (TOMBO): Concept and experimental verification. *Applied Optics*, 40(11), 1806–1813.

## Biographical sketches



**Edmund Y. Lam** received the B.S. degree (with distinction) in 1995, the M.S. degree in 1996, and the Ph.D. degree in 2000, all in electrical engineering from Stanford University, Stanford, CA. At Stanford, he developed image processing algorithms for the Programmable Digital Camera project. He also consulted for industry in the areas of digital camera systems design and algorithms development. Before returning to academia, he was affiliated with the Reticle and Photomask Inspection Division (RAPID) of KLA-Tencor Corporation in San Jose, CA, as a senior engineer, working in the design of defect detection tools for the core die-to-die and die-to-database inspections. He is currently an Assistant Professor of electrical and electronic engineering at the University of Hong Kong, as well as the Director of its Imaging Systems Laboratory. His research interests include electronic and computational imaging, and image processing applications in semiconductor manufacturing, biomedical engineering, and sensor networks. He is a senior member of IEEE and a member of SPIE.



**Giuseppe Y. Mak** received the B.Eng. (2002) and M.Phil. (2005) degrees in electrical and electronic engineering from the University of Hong Kong, Hong Kong, where he focused on aberration sensitivity reduction in microlithography. Later he worked as a research assistant and was involved in a project on computational imaging systems design. He is currently a product engineer in Brion Technologies, providing technical support to OPC verification software.



**Michael Ng** is a Professor in the Department of Mathematics at the Hong Kong Baptist University. As an applied mathematician, Michael's main research areas include Bioinformatics, Data Mining, Operations Research and Scientific Computing. Michael has published and edited 5 books, published more than 140 journal papers. He is the principal editor of the Journal of Computational and Applied Mathematics, and the associate editor of SIAM Journal on Scientific Computing.



**Wai-San Chan** received the B.Eng. degree in electrical and electronic engineering from the University of Hong Kong in 2005, where she is currently an M.Phil. candidate. Her research focus is in the field of computational imaging.